X-Ray Diffraction and Reflectivity Validation of the Depletion Attraction in the Competitive Adsorption of Lung Surfactant and Albumin

Patrick C. Stenger,[†] Guohui Wu,[†] Chad E. Miller,[§] Eva Y. Chi,[‡] Shelli L. Frey,[‡] Ka Yee C. Lee,[‡] Jaroslaw Majewski,[§] Kristian Kjaer,[¶] and Joseph A. Zasadzinski[†*]

[†]Department of Chemical Engineering, University of California, Santa Barbara, California; [‡]Department of Chemistry, University of Chicago, Chicago, Illinois; [§]Los Alamos National Laboratory, Los Alamos, New Mexico; and [¶]Risø National Laboratory, Roskilde, Denmark

ABSTRACT Lung surfactant (LS) and albumin compete for the air-water interface when both are present in solution. Equilibrium favors LS because it has a lower equilibrium surface pressure, but the smaller albumin is kinetically favored by faster diffusion. Albumin at the interface creates an energy barrier to subsequent LS adsorption that can be overcome by the depletion attraction induced by polyethylene glycol (PEG) in solution. A combination of grazing incidence x-ray diffraction (GIXD), x-ray reflectivity (XR), and pressure-area isotherms provides molecular-resolution information on the location and configuration of LS, albumin, and polymer. XR shows an average electron density similar to that of albumin at low surface pressures, whereas GIXD shows a heterogeneous interface with coexisting LS and albumin domains at higher surface pressures. Albumin induces a slightly larger lattice spacing and greater molecular tilt, similar in effect to a small decrease in the surface pressure. XR shows that adding PEG to the LS-albumin subphase restores the characteristic LS electron density profile at the interface, and confirms that PEG is depleted near the interface. GIXD shows the same LS Bragg peaks and Bragg rods as on a pristine interface, but with a more compact lattice corresponding to a small increase in the surface pressure. These results confirm that albumin adsorption creates a physical barrier that inhibits LS adsorption, and that PEG in the subphase generates a depletion attraction between the LS aggregates and the interface that enhances LS adsorption without substantially altering the structure or properties of the LS monolayer.

INTRODUCTION

Adsorption of lung surfactants (LS) and many soluble proteins to the air-water interface occurs spontaneously because adsorption lowers the interfacial energy. The surface pressure, Π, is the negative derivative of the free energy, G, with respect to the interfacial area, A: $\Pi = -(\frac{\partial G}{\partial A})_n$. (1). The higher equilibrium surface pressure of LS (~45 mN/m (2)) compared with albumin (~20 mN/m (3)) suggests that LS should adsorb preferentially to albumin at an air-water interface. However, equilibrium says nothing about the relative adsorption rates. The rate of albumin adsorption from solution is favored by its nanometer size and subsequent faster diffusion compared with the multimicron bilayer liposomes of LS. In both the Langmuir trough and the expanding alveolus in the lung, a new air-water interface is continuously being created for this competitive adsorption. In addition to this new interface, for equilibrium to occur, LS must displace albumin from whatever part of the interface it occupies. However, LS adsorption, although favored energetically, does not occur for hours (if at all) when albumin is in the subphase or already occupies the interface (2,4). The transport of LS to the interface is inhibited by albumin at the interface, likely because of the energy barrier induced by the electrostatic and steric interactions between the anionic LS and the negatively charged albumin (4). This energy barrier to LS adsorption is directly analogous to the energy barrier that stabilizes colloidal dispersions and prevents them from flocculating (2,4–10). We and others (2,4–10) have found that oppositely charged polyelectrolytes and divalent ions, uncharged hydrophilic polymers, and increased total electrolyte concentration, all of which promote colloid flocculation, also promote LS displacement of albumin at interfaces.

One well-established method of flocculating colloids that also promotes surfactant adsorption is to add hydrophilic polymers, such as polyethylene glycol (PEG), to the surfactant dispersion (2,11,12). In analogy to their effects on colloids, polymers induce a ''depletion attraction'' between LS liposomes in solution and the interface (4,6,7). However, for the depletion attraction to exist, PEG must not adsorb to LS, albumin, or the air-water interface, i.e., there must be an excluded volume near the interface that the polymer is prevented from exploring. In previous work, we showed that the scaling of polymer concentration (6) and molecular weight (7) needed to restore surfactant adsorption is consistent with that predicted by the depletion attraction/energy barrier model (4). However, the molecular signatures of the depletion attraction require higher-resolution information from x-ray reflectivity (XR) (13,14) and grazing incidence x-ray diffraction (GIXD) to determine the location and organization of surfactant, protein, and polymer.

XR shows that when both Survanta (a clinical LS) and albumin are in the subphase, albumin dominates the interface. However, GIXD shows that small patches of LS coexist with the albumin, depending on the surface pressure. Adding

Submitted February 19, 2009, and accepted for publication May 5, 2009.

*Correspondence: gorilla@engineering.ucsb.edu

Editor: Huey W. Huang.

0006-3495/09/08/0777/10 $2.00

doi: 10.1016/j.bpj.2009.05.017

PEG to the subphase restores the characteristic LS isotherm even though albumin is also in the subphase. With PEG, the average electron density and Bragg peaks are similar to those of Survanta on a pristine subphase, confirming that the Survanta has displaced the albumin at the interface. XR also shows that PEG is depleted from the interface, consistent with the depletion attraction mechanism. It was previously suggested that albumin and/or PEG might alter the molecular ordering of an LS film at the air-water interface (15), resulting in a hybrid surfactant/albumin mixed film at the air-water interface (10,15,16). However, GIXD shows that the molecular organization of the ordered fraction of the Survanta film is substantially unchanged by PEG or albumin at all surface pressures, although GIXD cannot address the molecular organization of the disordered fraction of the monolayer.

MATERIALS AND METHODS

Survanta is a clinical replacement LS prepared by organic extraction of minced bovine lungs (Abbott Laboratories, Columbus, OH) (17) and was a generous gift of the Santa Barbara Cottage Hospital nursery. NaCl, $CaCl_2$, $NaHCO_3$, 10 kDa PEG, and bovine serum albumin were obtained from Sigma (St. Louis, MO) and used as received. All water used in experiments had a resistivity of 18.2 MΩ-cm (Millipore gradient system; Millipore, Billerica, MA). All synchrotron x-ray measurements were carried out using the liquid surface diffractometer at the BW1 (undulator) beam line at the Hamburg Synchrotron Radiation Laboratory, German Electron Synchrotron (Hamburg, Germany). The theory of XR and GIXD has been presented in detail elsewhere (13,18,19) and the scattering geometries used have also been illustrated previously (19,20). A temperature-controlled Langmuir trough equipped with a Wilhelmy plate and motorized barrier was mounted on the diffractometer and maintained at 20°C. After the samples were prepared, but before x-ray data were collected, helium was flushed through the trough enclosure for at least 40 min to reduce the scattering background and to minimize beam damage during x-ray scans. The oxygen level was constantly monitored to be <2%. The synchrotron x-ray beam was monochromated to a wavelength of λ ~1.304 Å by Bragg reflection from a Beryllium (200) monochromator crystal in the Laue geometry. To initiate each experiment, an albumin and/or polymer containing buffer (150 mM NaCl, 2 mM $CaCl_2$, 0.2 mM $NaHCO_3$, pH 7) in the Langmuir trough was allowed to equilibrate for 10 min; for albumin-containing subphases, Π increased to ~18 mN/m. Survanta was diluted in the same buffer to a lipid concentration of 2 mg/mL and deposited as microliter drops from a syringe by touching the drop to the air-water interface of the open trough. The subphase was not stirred, and the first compression began 20 min after deposition.

For GIXD, the x-ray beam is configured to strike the surface at an incident angle of 0.11°, which corresponds to $q_z = 0.85\ q_c$, where $q_c = 0.0219$ Å^{-1} is the critical scattering vector for total external reflection from the subphase. At this angle, the incident wave is totally reflected, whereas the refracted wave is an evanescent wave traveling along the liquid surface. Such a configuration maximizes surface sensitivity. The dimension of the x-ray beam footprint on the liquid surface was ~2 mm × 50 mm. For in-plane diffraction measurements, a Soller collimator (JJ X-ray, Liseleje, Denmark) consisting of closely spaced vertical plates was placed before a vertical, one-dimensional, position-sensitive detector with vertical acceptance $0 < q_z < 1.2$ Å^{-1}, yielding a lateral resolution of $\Delta q_{xy} = 0.0084$ Å^{-1}. As a precaution against beam damage, the trough was translated perpendicular to the x-ray beam at every step of the q_{xy} scan. The Origin Peak Fitting Module (Northampton, MA) was used to fit the Bragg peaks. After the number of peaks was specified, the fit with the lowest χ^2 was chosen. GIXD provides information only about ordered domains within the monolayer; disordered regions do not diffract appreciably (19).

The reflectivity, R, is defined as the ratio of the intensity of x rays specularly reflected from a surface relative to that of the incident x-ray beam. When measured as a function of wave-vector transfer ($q_z = |k_{out} - k_{in}| = 4\pi\sin\alpha/\lambda$, where α is the grazing angle and λ is the wavelength of the x-ray beam), the reflectivity curve contains information on the sample-normal profile of the in-plane average of the electron density. Reflectivities with q_z values from 0.01 to 0.8 Å^{-1} were measured using an NaI scintillation detector, and reasonable statistics were obtained for values of $R \geq 10^{-10}$. Typical scanning times for this q_z range were 30 min. As a precaution against beam damage, the sample was regularly translated for the full 2-mm width of the beam. Remeasuring part of the reflectivity curve before and after translation afforded a check of the reproducibility. The absolute reflectivity was derived by subtracting the measured background, followed by normalization to the incident beam flux. The data were plotted as R/R_F versus the perpendicular scattering vector, q_z. The error bars on the data represent the statistical errors in the measurements (standard deviation, $\pm\sigma_R$). The measured reflectivity curves were analyzed using a model-free approach (21–23) to obtain detailed information on the electron density distribution in the direction normal to the interface. Increasing z represents moving from the air through the monolayer and into the subphase. For comparison, all electron density curves were aligned vertically at the tailgroup inflection point, which was set at $z = 7.7$ Å.

RESULTS

GIXD

Fig. 1 shows the Bragg peaks (Fig. 1 *a*) and Bragg rods (Fig. 1 *b*) from a Survanta film on the control subphase. At 20 mN/m, two Bragg peaks are present, with the integrated intensity of the $q_{xy} = 1.44$ Å^{-1} or {1,0} peak roughly twice that of the $q_{xy} = 1.48$ Å^{-1} or {1,1} peak, indicating a distorted hexagonal lattice similar to DPPC and DPPC/palmitic acid (PA) mixtures under similar conditions (24,25). The measured lattice spacings ($d_{xy} = 2\pi/q_{xy}$), $d_{10} = 4.38$ Å and $d_{11} = 4.24$ Å, correspond to a distorted hexagonal unit cell with axes $a_H = 4.95$ Å and angle γ=118°. The area per hydrocarbon chain (phospholipids are composed of two alkyl chains and PA of one alkyl chain per molecule, respectively) is 21.7 Å^2, similar to DPPC, DPPC/PA (24,25), and previous measurements of Survanta (26). The Bragg rod profile (Fig. 1 *b*) exhibits a local maximum at $q_z = 0.41$ Å^{-1}, indicating that the lipid molecules are tilted relative to the surface normal (26).

Increasing the surface pressure to 30 mN/m causes the two Bragg peaks to shift to $q_{10} = 1.47$ Å^{-1} and $q_{11} = 1.49$ Å^{-1} indicating a more compact distorted hexagonal lattice. The Bragg rod profile exhibits a local maximum at $q_z = 0.23$ Å^{-1}, indicating a reduction in lipid tilt with increasing surface pressure commensurate with the smaller area per hydrocarbon chain (25). At 40 mN/m, the single peak at $q_{10} = 1.49$ Å^{-1} indicates a transition to an untilted hexagonal lattice with $d_{10} = 4.21$ Å and $a_H = 4.86$ Å. The Bragg rod shows no local maximum, indicating that the lipid molecules are normal to the interface. In addition to the main peak, there is a small peak at $q_{xy} = 1.42$ Å^{-1} for $\Pi \geq 40$ mN/m, which likely corresponds to a minor fraction of a second crystalline phase (26). The origin of this second phase is unknown; Survanta contains small fractions of saturated lipids in addition to

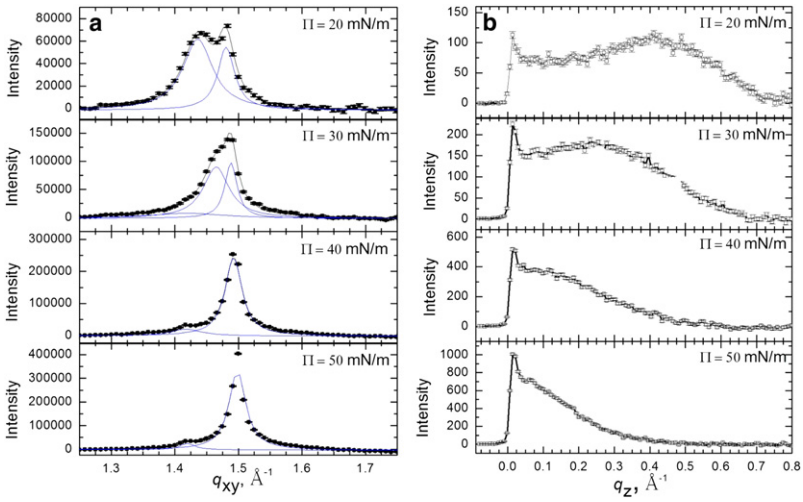

FIGURE 1 Bragg peaks and rods from GIXD of 200 μg Survanta spread onto a saline buffer subphase. (*a*) Bragg peaks at 20–50 mN/m. (*b*) Bragg rods at 20–50 mN/m.

DPPC capable of forming crystalline phases (17). Increasing the surface pressure to 50 mN/m results in only a slight shift of the main peak to $q_{xy} = 1.50$ Å^{-1}; the Bragg rods again indicate that the molecules are untilted. In contrast to the well-defined lattice of Survanta films, GIXD scans of subphases containing 2 mg/mL albumin, 5% wt. PEG, or mixtures of albumin and PEG, lack the Bragg peaks indicative of long-range order over the q_{xy} ranges for phospholipid films or proteins (data not shown).

Fig. 2 shows the Bragg peaks (Fig. 2 *a*) and Bragg rods (Fig. 2 *b*) from GIXD of Survanta on a subphase containing 5% wt. PEG. For $\Pi = 25$ mN/m (with PEG, the minimum surface pressure of the Survanta film was $>$ 20 mN/m; Fig. 1 *c*), the two Bragg peaks with $q_{10} = 1.44$ Å^{-1} and $q_{11} = 1.48$ Å^{-1} with a 2:1 integrated intensity are identical to the distorted hexagonal lattice of Survanta on the control subphase. The Bragg rod profile exhibits a local maximum at $q_z = 0.41$ Å^{-1}, indicating that the lipid molecules are tilted. At $\Pi = 30$ mN/m, the two Bragg peaks shift right to $q_{10} = 1.45$ Å^{-1} and $q_{11} = 1.49$ Å^{-1} and the Bragg rod maxima moves to $q_z = 0.35$ Å^{-1}, indicating a reduction in tilt and a more compact lattice. At 40 mN/m, a single peak is present at $q_{10} = 1.50$ Å^{-1}, indicating a transition to hexagonal packing. The Bragg rod at $q_{10} = 1.50$ Å^{-1} shows no local maximum, indicating that the molecules are normal to the interface. As was the case for Survanta with no PEG, a smaller peak occurs at $q_{xy} = 1.42$ Å^{-1}, indicative of a second crystalline phase. The peak positions at $q_{10} = 1.50$ Å^{-1} and $q_{xy} = 1.42$ Å^{-1} are unchanged at 50 mN/m.

Fig. 3 shows the Bragg peaks from GIXD scans of 600 μg Survanta spread on a 2 mg/mL albumin subphase (see the Supporting Material). At $\Pi = 20$ mN/m, different areas of the interface showed different scattering. Region 1 (*top panel*) shows no diffraction peaks consistent with albumin at the interface. However, region 2 (second panel, obtained by moving the sample horizontally by several millimeters in the direction perpendicular to the beam) shows diffraction peaks consistent with a distorted hexagonal lattice with $q_{10} = 1.39$ Å^{-1} and $q_{11} = 1.47$ Å^{-1}. The lattice is somewhat expanded compared to Survanta at 20 mN/m with $a_H = 5.04$ Å and γ=116°. The Bragg rods (not shown) exhibit a local maximum at $q_z = 0.57$ Å^{-1}, indicating a greater molecular

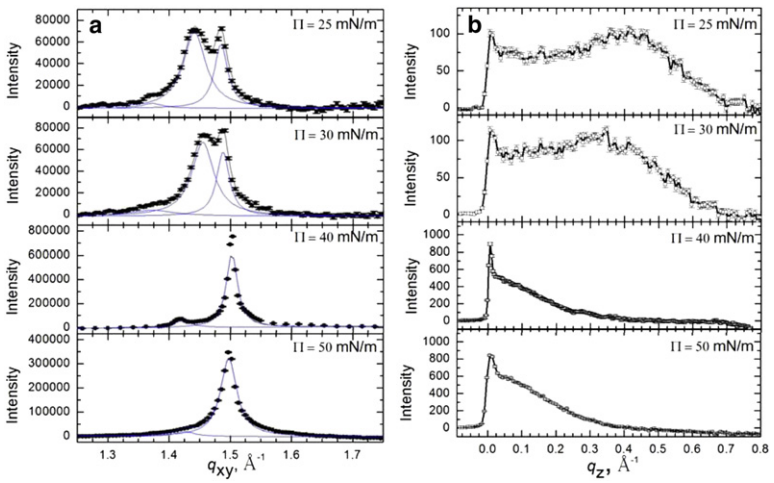

FIGURE 2 Bragg peaks and rods from GIXD of 200 μg Survanta spread onto a saline buffer subphase containing 5% wt. PEG. (*a*) Bragg peaks at 25–50 mN/m (The minimum surface pressure was ~25 mN/m on the PEG subphase. (*b*) Bragg rods at 25–50 mN/m. Both the Bragg peaks and rods are similar to those of Survanta on the control subphase.

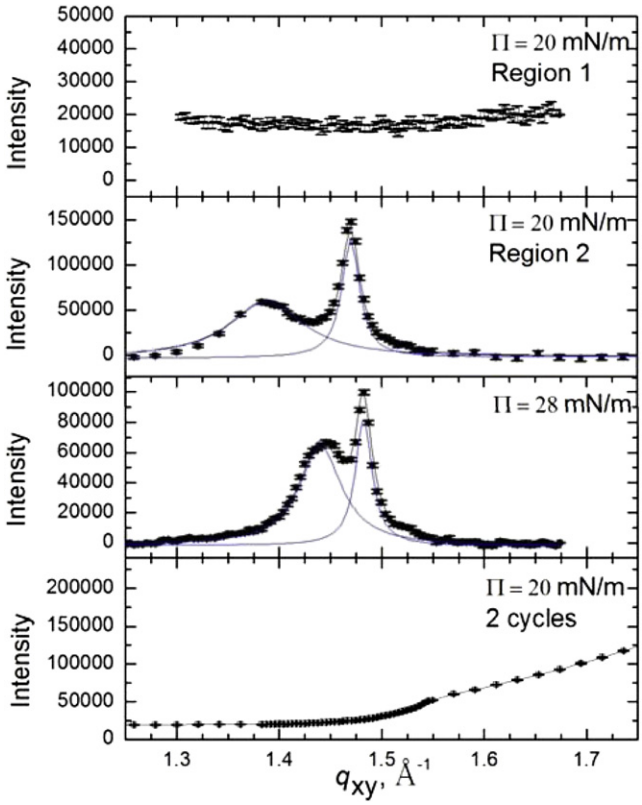

FIGURE 3 Bragg peaks from GIXD of 600 μg Survanta spread onto a saline buffer subphase containing 2 mg/mL albumin. The first two panels show different regions of the film at the same surface pressure. The top panel shows no Bragg peaks in region 1, consistent with an albumin-covered interface. The second panel shows that in the adjacent region (region 2), Bragg peaks reveal the presence of Survanta. The third panel shows that the Survanta lattice compacts with increasing surface pressure; however, surface pressures higher than 28 mN/m could be sustained due to the presence of albumin. The last panel shows GIXD at 20 mN/m after two additional cycles; the Survanta peaks are no longer present.

tilt than Survanta on the control subphase (Fig. 1 *b*). The diffraction peaks demonstrate that some ordered domains of Survanta are present at the interface. Increasing the surface pressure to the maximum sustainable under these conditions (28 mN/m), causes the two peaks to shift to $q_{10} = 1.44$ Å^{-1} and $q_{11} = 1.48$ Å^{-1}, corresponding to a less tilted and more compact distorted hexagonal lattice. The local maximum at $q_z = 0.37$ Å^{-1} indicates a greater molecular tilt than Survanta on the control subphase at the same surface pressure (see Table 1). As the tilt and the lattice spacing of Survanta and other lipids increases with decreasing surface pressure (14,24–27), the albumin acts as if it were lowering the effective surface pressure that the Survanta experiences. The last panel in Fig. 3 shows GIXD scans after two additional compression-expansion cycles; the Bragg peaks can no longer be found, indicting that no ordered domains of Survanta remain at the interface.

Bragg peaks (Fig. 4) from GIXD scans of 600 μg Survanta spread on a subphase with 2 mg/mL albumin and 5% wt. PEG confirm the adsorption of Survanta. Before the Survanta was spread, the surface pressure was ~18 mN/m, indicating albumin had adsorbed to the interface. However, after the Survanta was spread, the characteristic Survanta diffraction peaks were observed everywhere on the interface. At 20 mN/m, $q_{10} = 1.48$ Å^{-1} and $q_{11} = 1.49$ Å^{-1}; the Bragg rods have a local maximum at $q_z = 0.09$ Å^{-1} (not shown). Compared to Survanta at 20 mN/m, the PEG in the subphase condenses the Survanta lattice and reduces the tilt. By 30 mN/m, the lattice has further condensed with $q_{10} = 1.50$ Å^{-1} and $q_z = 0$ Å^{-1}, indicating that the molecules are hexagonally packed and normal to the interface. At 40 mN/m, the main peak remains at $q_{xy} = 1.50$ Å^{-1} and a smaller peak remains at $q_{xy} = 1.45$ Å^{-1}, indicating that a second crystalline phase is also present. This second phase is shifted compared to Survanta at 40 mN/m, indicating a slightly tighter packing due to the effects of the PEG. The Bragg rods show no local maximum ($q_z = 0$ Å^{-1}) at 40 mN/m, indicating that the molecules are normal to the interface.

X-ray reflectivity

XR provides an averaged electron density profile normal to the interface of all lipid and protein components, which complements the in-plane information from GIXD. Fig. 5 *a* shows the reflectivity, R, scaled by the Fresnel reflectivity, R_F, for Survanta spread on the control subphase; the corresponding electron density profiles, normalized by the subphase electron density ($\rho(z)/\rho_{sub}$) are shown in Fig. 5 *b* (21–23). (The double cusp of R/R_F near $q_z = 0.02$ Å^{-1} is a visual artifact that comes from dividing the measured $R(q_z)$, which is affected by finite resolution by the ideally calculated Fresnel law $R_F(q_z)$). For the Survanta films, the electron density begins at 0 on the air side of the interface ($z = 0$), rises sharply through the tail region, and reaches a maximum at the headgroup region at $z \sim 30$ Å before quickly decaying to the subphase electron density ($\rho(z)/\rho_{sub} = 1$) at $z \sim 42$ Å. All data sets were fit over a z range from 0 to 140 Å to facilitate comparisons between samples. Care was taken to ensure that increasing the range of z did not significantly change the χ^2 of the fit or the shape of the electron density curves for the electron density profiles that did not contain albumin and did not show deviations from the water electron density for $z > 50$ Å. The density of the headgroup maximum increases (from 1.17 to 1.22) and the width of the maximum decreases and shifts to the right with increasing surface pressure, indicating a reduction in the tilt of the tails, consistent with the Bragg rods in Fig. 1 and previous XR of DPPC monolayers (29).

Fig. 6, *a* and *b*, show XR and electron density profiles for a 2 mg/mL albumin-containing subphase as well as 600 μg Survanta spread on the albumin subphase. The electron density at the interface increases more sharply than does Survanta on the control subphase (Fig. 5 *b*), reaching a maximum $\rho/\rho_{sub} = 1.25$ at $z = 15$ Å. Unlike the electron density

TABLE 1 Survanta *d*-spacings, unit cell parameters, coherence length, and area per chain as a function of subphase composition and surface pressure

			Phase 1					Phase 2			
Subphase	π, mN/m	Packing	Observed *d*-spacing d_{10} (Å)	Observed *d*-spacing $d_{1\text{-}1}$ (Å)	Unit cell a=b (Å)	Angle α	Coherence length L^c_{10} (Å)	Coherence length $L^c_{1\text{-}1}$ (Å)	Area per chain (A^2)	Observed *d*-spacing d_{10} (Å)	Unit cell $a = b$ (Å)
Saline buffer	20	Dist. Hex	4.38	4.24	4.95	118	100	175	21.7	—	-
Saline buffer	30	Dist. Hex	4.29	4.22	4.90	119	115	265	21.0	4.43	5.12
Saline buffer	40	Hexagonal	4.21	—	4.86	120	177	—	20.5	4.43	5.12
Saline buffer	50	Hexagonal	4.19	—	4.84	120	185	—	20.3	4.43	5.12
PEG	25	Dist. Hex	4.36	4.23	4.94	118	129	225	21.5	4.58	5.29
PEG	30	Dist. Hex	4.32	4.22	4.91	118	131	237	21.2	4.58	5.29
PEG*	40[a]	Hexagonal	4.18	—	4.83	120	287	—	20.2	4.42	5.10
PEG*	40	Hexagonal	4.19	—	4.83	120	200	—	20.2	4.42	5.10
PEG	50	Hexagonal	4.20	—	4.84	120	181	—	20.3	4.41	5.09
Albumin	20	Dist. Hex	4.53	4.28	5.04	116	64	296	22.8	—	—
Albumin	30	Dist. Hex	4.36	4.24	4.94	118	113	312	21.6	—	—
Albumin/PEG	20	Dist. Hex	4.25	4.21	4.88	119	183	399	20.7	4.57	5.28
Albumin/PEG	30	Hexagonal	4.19	—	4.84	120	494	—	20.3	—	—
Albumin/PEG	40	Hexagonal	4.18	—	4.83	120	280	—	20.2	4.33	5.00

Values are calculated from peak positions of the in-plane scattering vector component q_{xy} from peak fits using a Lorentzian model. Phase 1 is the dominant phase and transitions from a distorted hexagonal lattice ($a = b$, $\alpha \neq 120°$) to a hexagonal lattice ($a = b$, $\alpha = 120°$) with increasing surface pressure. Phase 2 d-spacings are given only for experiments in which the signal is above the background. The phase 2 lattice is assumed to be hexagonal.
*First row for a PEG subphase at 40 mN/m is 200 μg Survanta, and the second is 600 μg.

profiles for Survanta (Fig. 5 *b*), ρ/ρ_{sub} is significantly greater than one for $50 < z < 100$ Å. The error (χ^2) of the fit of the XR data on the albumin subphase increased significantly when the length of the electron density profile was reduced from $z = 140$ Å. A Fourier transform of the XR data (see the Supporting Material) shows peaks above the noise at

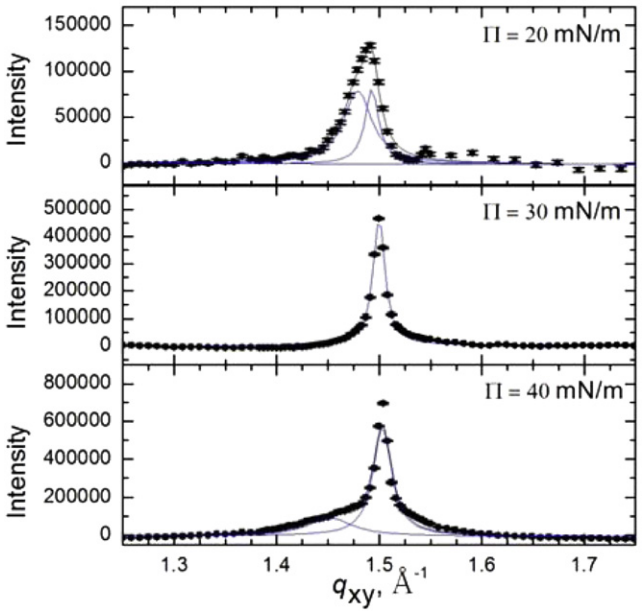

FIGURE 4 Bragg peaks from GIXD of 600 μg Survanta spread onto a subphase containing 2 mg/mL albumin and 5% wt. PEG at 20–40 mN/m. The packing changes from distorted hexagonal to hexagonal at a lower surface pressure than Survanta on the control subphase. The hexagonal lattice with zero tilt occurs at a lower surface pressure than on the control subphase (Fig. 1).

$z \sim 50$ Å and 85 Å, suggesting a second layer of albumin, which is a prolate spheroid of dimensions 40 × 40 × 140 Å (30). Both neutron reflectivity (30) and ellipsometry (31) of albumin at the air-water interface also indicate a dense, closely packed monolayer followed by a less dense second layer. Our XR data indicate two layers with the albumin long axis parallel to the interface. Other globular proteins, such as β-lactoglobulin, have a similar maximum electron density ($\rho/\rho_{sub} = 1.20$) (32).

The electron density (Fig. 6 *b*) in regions 1 and 2 (defined in Fig. 3) is qualitatively similar to that of albumin, even though GIXD showed small patches of ordered Survanta in region 2. However, the electron density of the mixed Survanta/albumin films in both regions 1 and 2 decreased more quickly with increasing z than the albumin film. This suggests that Survanta has displaced the second layer of albumin. In contrast, the electron density of the mixed Survanta-albumin film at 28 mN/m, the highest surface pressure that can be sustained for the duration of the XR experiment, overlays that of Survanta on the control buffer at 30 mN/m. The GIXD curve of Survanta-albumin at 28 mN/m (Fig. 4) shows diffraction peaks, confirming that Survanta is at the interface. The ratio of Survanta to albumin at the interface apparently increases with increasing surface pressure. However, the film is still ''inhibited'' by albumin; isotherms (Supporting Material) show that the maximum surface pressure does not increase above 35 mN/m even after compression to the smallest trough area, suggesting that the Survanta never completely displaces the albumin.

Fig. 7, *a* and *b*, show the XR and electron density profiles for low (200 μg) and high (600 μg) concentrations of Survanta spread on a subphase containing 5% wt. PEG at

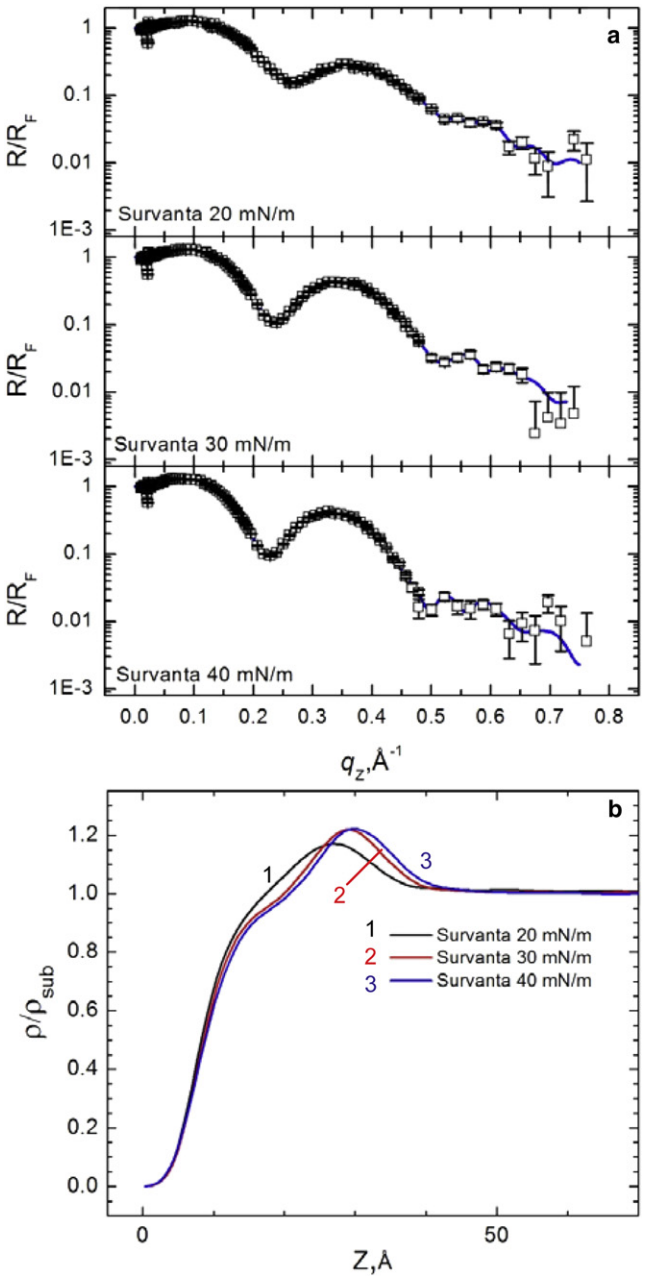

FIGURE 5 (*a*) XR for 200 μg Survanta spread on the control subphase. The blue lines are fits to the data using a model-independent algorithm as discussed in the text. (*b*) The electron density profiles, normalized by the subphase electron density, for the corresponding XR data. With increasing surface pressure, the headgroup maximum increases, the width of the headgroup region decreases, and the location of the headgroup maximum shifts to the right.

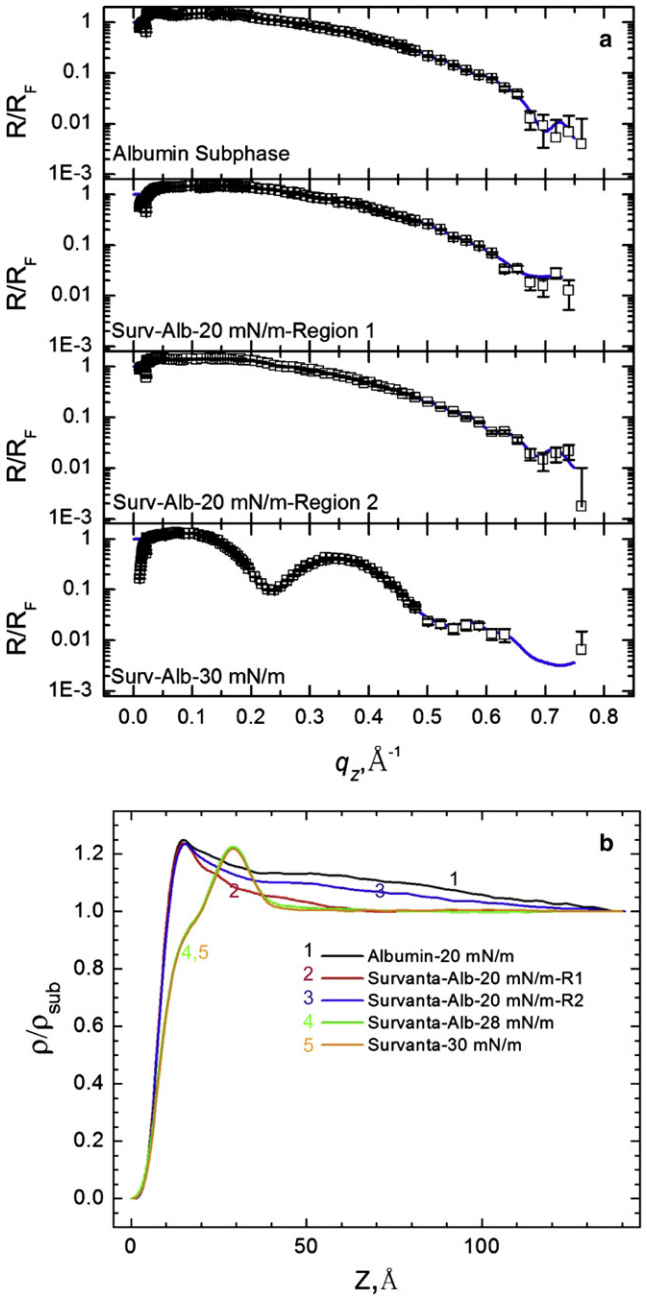

FIGURE 6 (*a*) XR for 600 μg Survanta spread on a saline buffer subphase containing 2 mg/mL albumin. No Survanta is present for the albumin subphase data. Regions 1 and 2 are the same areas used for the GIXD in Fig. 4. (*b*) The electron density profiles, normalized by the subphase electron density. For Survanta-albumin-20 mN/m, the electron density profile is similar to that of albumin for both regions 1 and 2, whereas at 28 mN/m the electron density profile is similar to that of Survanta (Fig. 6).

40 mN/m. PEG increases the subphase electron density ~6% and this value ($\rho_{sub} = 0.353$ e$^-$/Å^3) was used for all XR fits. Fig. 7 *b* shows that ρ/ρ_{sub} is less than unity for the PEG-containing subphase over the entire range of z, with a minimum value of 0.98. This suggests that the PEG concentration near the interface is below that of the bulk, consistent with a PEG ''depletion layer'' at the interface (4). The ρ/ρ_{sub} values for both low (200 μg) and high (600 μg) Survanta concentrations on the PEG subphase at 40 mN/m are identical; the electron density reaches a maximum of $\rho/\rho_{sub} = 1.11$. The agreement between the XR curves at different concentrations is consistent with the GIXD results (Table 1), which shows that both the lateral and vertical surfactant organizations

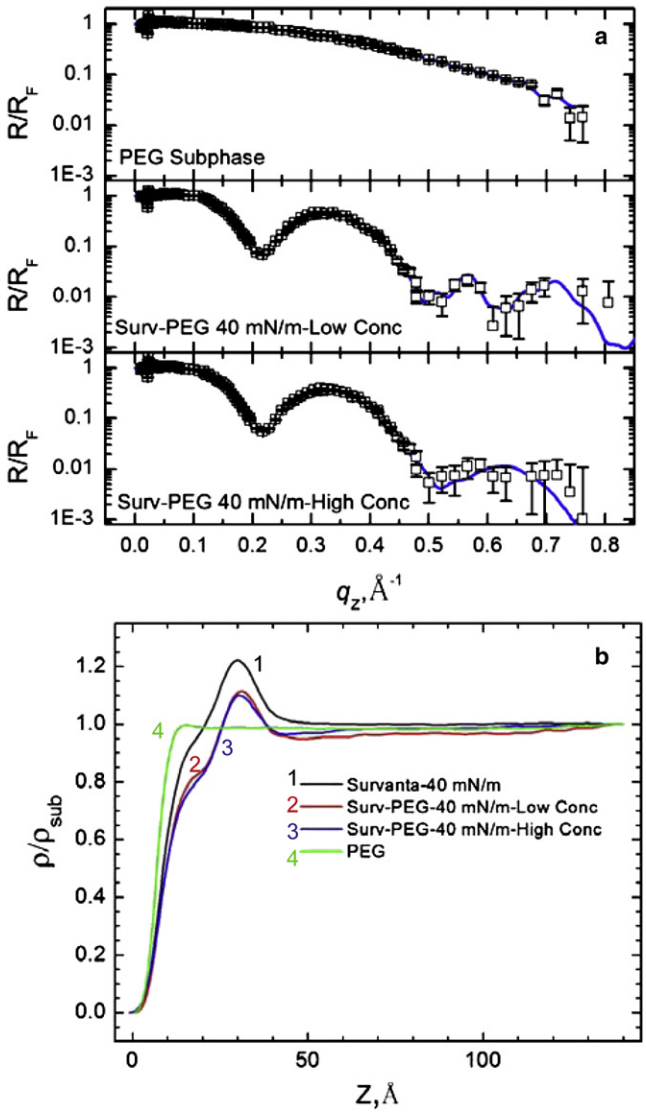

FIGURE 7 (*a*) XR for 200 μg and 600 μg of Survanta spread on a saline buffer subphase containing 5% wt. PEG at 40 mN/m. No Survanta is present for the PEG subphase data. (*b*) The electron density profiles, normalized by the subphase electron density. The two Survanta concentrations result in nearly identical density profiles. The electron density profile of 200 μg Survanta on the control subphase at 40 mN/m is shown for comparison.

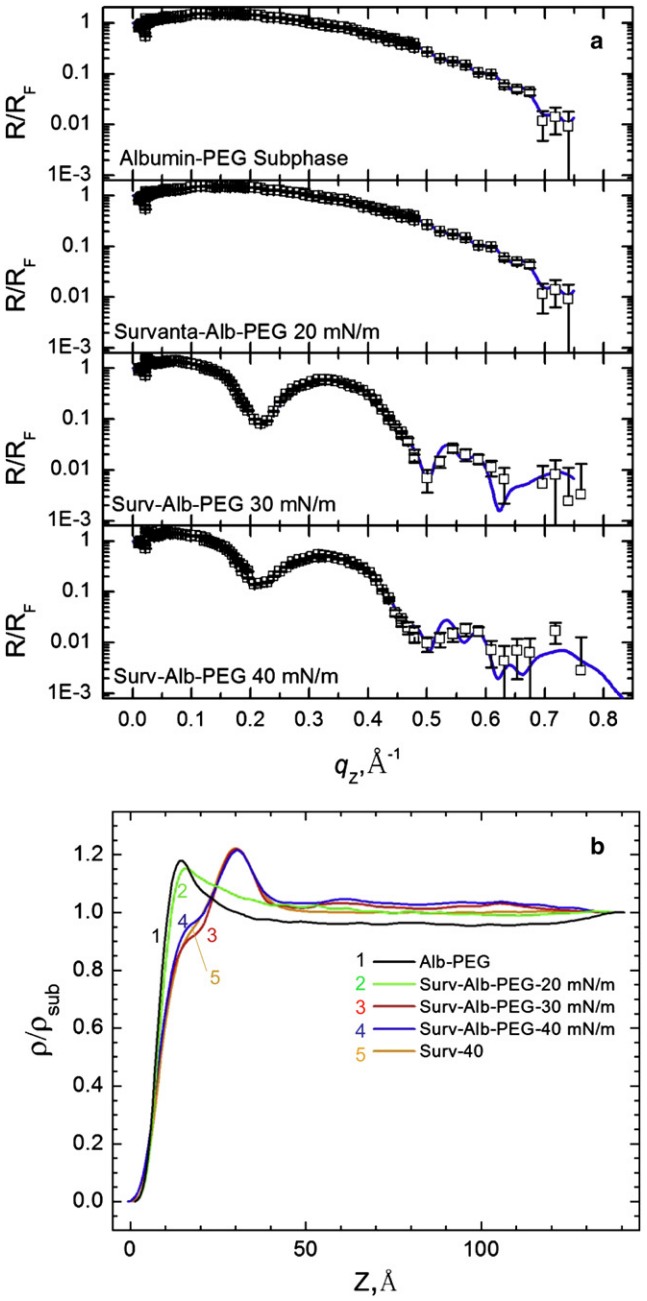

FIGURE 8 (*a*) XR for 600 μg Survanta spread on a subphase containing 2 mg/mL albumin and 5% wt. PEG. No Survanta is present for the albumin-PEG subphase data. (*b*) The electron density profiles normalized by the subphase electron density. At 20 mN/m, the electron density profile is similar to that of albumin, whereas for 30 and 40 mN/m, the electron density is similar to that of Survanta, indicating that Survanta has displaced the albumin. The electron density profile of 200 μg Survanta on the control subphase at 40 mN/m is shown for comparison.

are independent of subphase concentration. The electron density at the interface drops below unity for both concentrations, reaching a minimum value of 0.95 for the high concentration, which is also consistent with a PEG depletion layer. The maximum in ρ/ρ_{sub} corresponding to the headgroups, and the inflection at $z \sim 19$ Å corresponding to the tailgroups are reduced on the PEG subphase compared to the control buffer; the headgroup maximum ρ/ρ_{sub} decreases from 1.22 to 1.11, and the tailgroup ρ/ρ_{sub} decreases from 0.96 to 0.82.

Fig. 8, *a* and *b*, show the XR and electron density profiles for Survanta spread on a subphase containing both 2 mg/mL albumin and 5% wt. PEG. The albumin-PEG subphase has an electron density profile similar to that of albumin (Fig. 6), with a maximum electron density of $\rho/\rho_{sub} = 1.18$ at $z = 15$ Å. However, the albumin-PEG subphase profile decreases more quickly than albumin and reaches a minimum value of 0.95, again consistent with a PEG depletion layer.

For Survanta on an albumin-PEG subphase at 20 mN/m, the electron density profile is qualitatively similar to that of albumin for $z < 50$ Å, indicating that the interfacial film within the beam footprint is dominated by albumin. However, GIXD for the same film at 20 mN/m (Fig. 4) shows diffraction peaks, indicating that some ordered Survanta coexists at the interface. The Survanta-albumin-PEG 20 mN/m electron density profile decreases less quickly than that for the albumin-PEG subphase; for $z > 50$ Å, it overlaps with the Survanta electron density profile. For Survanta-albumin-PEG at 30 mN/m and 40 mN/m, the electron density profiles are more similar to that of Survanta on the control subphase, indicating that at higher surface pressures, Survanta has displaced albumin from the interface. However, $\rho/\rho_{sub} > 1$ at larger z, which may be due to albumin remaining near the interface. The magnitude of this effect may be masked by the PEG depletion layer. Overall, when PEG and albumin are in the subphase, XR and GIXD show that the Survanta displaces albumin from the subphase as the surface pressure increases.

DISCUSSION

Table 1 summarizes the area per hydrocarbon chain of the in-plane ordered fraction of Survanta as a function of subphase composition and surface pressure. The projected area per chain normal to the interface decreases with increasing surface pressure for all subphases. The area/molecule for the control interface changes from 21.7 Å^2 at 20 mN/m to 20.3 Å^2 at 50 mN/m, primarily due to the decreasing molecular tilt. GIXD shows that when Survanta coexists with albumin at the interface without PEG in the subphase, the area per chain increases to 22.8 Å^2 at 20 mN/m. Albumin seems to lower the effective surface pressure, allowing the Survanta lattice to tilt more than on the control subphase. On the other hand, PEG compacts the Survanta lattice; the area per chain decreases from 21.7 Å^2 (control) to 20.7 Å^2 (albumin-PEG) at 20 mN/m, again by decreasing the molecular tilt. By 40 mN/m, the lattice is hexagonal and the molecules are untilted on all subphases, and the area per chain on the albumin-PEG subphase is identical to the PEG subphase (20.2 Å^2), and only slightly less than on the control subphase (20.5 Å^2). At low surface pressures, where the molecules are tilted, PEG and albumin together in the subphase have the same effect on Survanta as increasing the surface pressure by ~10 mN/m; albumin alone has the same effect as decreasing the surface pressure by ~5 mN/m. Once the molecules are normal to the interface, there is less change in the area/molecule by PEG or albumin, or by further increases in the surface pressure.

The lattice spacing and tilt of the main diffraction peaks and their evolution with surface pressure are consistent with the ordered domains of Survanta being composed of DPPC (~70% wt.) and the PA that is added to the bovine extract (PA ~10% wt.) (17,24–26). Previous work has shown that the unsaturated lipids along with the SP-B and SP-C proteins separate into the disordered phases and hence do not contribute to the diffraction peaks (25,33–35). GIXD of a DPPC/POPG/PA (69/20.5/10 wt.) lipid mixture on a pure water subphase shows that the lattice changes from tilted, oblique lattice at 25 mN/m with $d_{10} = 4.38$ Å, $d_{01} = 4.30$ Å, and $d_{11} = 4.23$ Å to a simple hexagonal lattice at 50 mN/m with $d_{10} = 4.17$ Å (25). For the DPPC/POPG/PA mixture, the tilt is reduced from 19° at 25 mN/m to 0° at 50 mN/m. Survanta has a tilted, distorted hexagonal lattice with $d_{10} = 4.38$ Å and $d_{11} = 4.24$ Å at 20 mN/m, and compacts to an untilted hexagonal lattice with $d_{10} = 4.19$ Å at 50 mN/m. The similarity between the evolution of the molecular organization with surface pressure and the details of the lattice spacing of the simple lipid mixtures suggest that the solid phase in Survanta is composed mainly of DPPC and PA (26). The presence of a second, minor crystalline phase in Survanta is not unexpected in a complex mixture; our previous limited GIXD study on Survanta also showed two phases (26).

Albumin has similar effects on the Survanta film as Poloxamer 188 (P188), a triblock copolymer with a polyethylene oxide-polypropylene oxide-polyethylene oxide structure (molecular weight: 8400) has on DPPC (29,36). Both albumin and P188 are water-soluble and surface-active (29,36). At 30 mN/m, the Bragg peaks for DPPC ($q_{10} = 1.38$ Å^{-1}, $q_{11} = 1.46$ Å^{-1}) and DPPC/P188 ($q_{10} = 1.37$ Å^{-1}, $q_{11} = 1.46$ Å^{-1}) monolayers are nearly identical. P188 is squeezed out of the interfacial film at surface pressures of 35–40 mN/m, which is ~15 mN/m above its equilibrium surface pressure. At pressures below 35–40 mN/m, XR shows a heterogeneous film that contains P188-rich and DPPC-rich regions; above 40 mN/m, GIXD shows that the film is identical to DPPC. In contrast, at 28 mN/m, the Bragg peaks for Survanta on an albumin subphase ($q_{10} = 1.44$ Å^{-1}, $q_{11} = 1.48$ Å^{-1}) are slightly shifted compared to Survanta on the control subphase at 30 mN/m ($q_{10} = 1.47$ Å^{-1}, $q_{11} = 1.49$ Å^{-1}), with a similar trend at 20 mN/m. XR shows that albumin and Survanta coexist on an albumin-containing subphase, with a gradual transition from albumin-rich at low surface pressure to Survanta-rich at higher surface pressures. Fluorescence images show that patches of albumin can coexist with Survanta at surface pressures as high as 55–60 mN/m (5–7). This is significantly higher than the albumin equilibrium surface pressure of 18 mN/m; albumin deviates significantly from ideal Gibbs monolayer behavior despite its molecular solubility. Albumin, unlike P188, has secondary and tertiary structures that can denature at the interface, which is likely the origin of this nonideal behavior at the interface (31). Although the primary effect of the albumin is to inhibit Survanta from reaching the interface, albumin also acts to lower the effective surface pressure at the interface, resulting in a less-compact, less-ordered Survanta film.

When PEG and albumin are present together in the subphase at 20 mN/m, GIXD shows diffraction peaks,

whereas XR shows an electron density similar to that of albumin, indicating that the interface is albumin-rich. However, albumin is displaced from the interface at higher surface pressures; at 30 and 40 mN/m, GIXD shows Survanta peaks, whereas XR shows a Survanta-like average electron density. This heterogeneity of the Survanta-albumin interface on the scale of the x-ray footprint is consistent with previous fluorescence images of the interface (5–7). Only when sufficient Survanta adsorbs to the interface at low surface pressures can the film achieve sufficiently high surface pressure on compression to ''squeeze out'' the albumin. These images show that under dynamic compression, some albumin remains up to a surface pressure as high as 55–60 mN/m. The measured electron density shows that the PEG concentration is lower at the interface than in the bulk, forming a ''depletion layer'', which is one of the requirements for a ''depletion attraction'' (4,6). PEG in the subphase compacts the Survanta lattice and eliminates the molecular tilt at a lower surface pressure compared to the control subphase. It may be that PEG induces a lateral ''depletion attraction'' within the film, as well as a depletion attraction that forces Survanta to the interface (37). More detailed GIXD measurements, especially on tilted and compressible monolayers as a function of PEG concentration, are needed to address this issue.

CONCLUSIONS

With increasing surface pressure, Survanta on a saline subphase, on a subphase with albumin, or on a subphase with albumin and PEG undergoes a transition from a distorted, tilted hexagonal lattice to an untilted hexagonal lattice with increasing surface pressure, in similarity to DPPC and DPPC/PA mixtures (24–27,36). XR confirms these results: the maximum in electron density associated with the headgroup increases, the width of the headgroup region decreases, and the location of the headgroup maximum indicates a reduction in the tilt of the monolayer with increasing surface pressure.

Adding 2 mg/mL albumin to the subphase inhibits Survanta adsorption to the interface indefinitely; only a small fraction of the interface shows Survanta diffraction peaks at 20 mN/m and the XR data show that the average electron density of the interface is that of albumin. The Survanta patches that do coexist with albumin have a larger lattice spacing and greater molecular tilt than on the control interface. Adding PEG to the albumin subphase restores the characteristic Survanta isotherms, and XR shows an average electron density similar to that of Survanta on the control subphase. The characteristic Survanta Bragg peaks are restored in the Survanta/albumin/PEG system, but with a slightly more compact lattice that undergoes the distorted hexagonal to hexagonal transition at a lower surface pressure. XR also shows that the PEG concentration is lower at the interface than in the bulk. This PEG depletion layer is consistent with the proposed depletion attraction/energy barrier model proposed to reverse LS inhibition (4). Our results confirm that negatively charged albumin at the interface inhibits adsorption of the negatively charged LS due to a combination of electrostatic and steric repulsion, analogously to the energy barriers that prevent colloid flocculation (4). Adding PEG induces a depletion attraction between the multimicron LS liposomes and the interface that decreases this repulsive energy barrier, leading to more Survanta reaching the interface. This increased LS adsorption then is capable of displacing albumin and maintaining higher surface pressures. Although this energy barrier-depletion attraction model has been used to explain isotherms, fluorescence microscopy images, and the scaling of adsorption with PEG concentration and molecular weight (6,7), the GIXD and XR data presented here directly show the three-dimensional distribution of albumin, PEG, and LS, confirming the molecular mechanisms of the model.

SUPPORTING MATERIAL

Text and one figure are available at http://www.biophysj.org/biophysj/supplemental/S0006-3495(09)01020-0.

We gratefully acknowledge beam time at the Hamburg Synchrotron Radiation Laboratory, German Electron Synchrotron, Hamburg, Germany.

This work was supported by National Institutes of Health grants HL-66410, HL-51177, and HL-080718. P.C.S. was partially supported by a National Science Foundation graduate research fellowship. J.M. and C.E.M. were supported by the Los Alamos National Laboratory under Department of Energy contract W7405-ENG-36 and by the Department of Energy Office of Basic Engineering Sciences. C.E.M. acknowledges support from the Los Alamos National Laboratory Director's Postdoctoral Fellowship and the Institute for Complex Adaptive Matter.

REFERENCES

1. Marsh, D. 1996. Lateral pressure in membranes. *Biochim. Biophys. Acta.* 1286:183–223.
2. Taeusch, H. W., J. Bernadino de la Serna, J. Perez-Gil, C. Alonso, and J. A. Zasadzinski. 2005. Inactivation of pulmonary surfactant due to serum-inhibited adsorption and reversal by hydrophilic polymers: experimental. *Biophys. J.* 89:1769–1779.
3. Warriner, H. E., J. Ding, A. J. Waring, and J. A. Zasadzinski. 2002. A concentration-dependent mechanism by which serum albumin inactivates replacement lung surfactants. *Biophys. J.* 82:835–842.
4. Zasadzinski, J. A., T. F. Alig, C. Alonso, J. Bernadino de la Serna, J. Perez-Gil, et al. 2005. Inhibition of pulmonary surfactant adsorption by serum and the mechanisms of reversal by hydrophilic polymers: theory. *Biophys. J.* 89:1621–1629.
5. Stenger, P. C., O. Palazolgu, and J. A. Zasadzinski. 2009. Mechanisms of polyelectrolyte enhanced surfactant adsorption at the air-water interface. *Biochim. Biophys. Acta.* 1788:1033–1043.
6. Stenger, P. C., and J. A. Zasadzinski. 2007. Enhanced surfactant adsorption via polymer depletion forces: a simple model for reversing surfactant inhibition in acute respiratory distress syndrome. *Biophys. J.* 92:3–9.
7. Stenger, P. S., S. G. Isbell, and J. A. Zasadzinski. 2008. Molecular weight dependence of the depletion attraction and its effects on the competitive adsorption of lung surfactant. *Biochim. Biophys. Acta.* 1778:2032–2040.
8. Yu, L. M. Y., J. J. Lu, I. W. Y. Chiu, K. S. Leung, Y. W. W. Chan, et al. 2004. Poly(ethylene glycol) enhances the surface activity of a pulmonary surfactant. *Coll. Surf. B. Biointerfaces.* 36:167–176.

9. Zuo, Y. Y., H. Alolabi, A. Shafiei, N. X. Kang, Z. Policova, et al. 2006. Chitosan enhances the in vitro surface activity of dilute lung surfactant preparations and resists albumin-induced inactivation. *Pediatr. Res.* 60:125–130.
10. Zuo, Y. Y., R. A. Veldhuizen, A. W. Neumann, N. O. Peterson, and F. Possmayer. 2008. Current perspectives in pulmonary surfactant—inhibition, enhancement and evaluation. *Biochim. Biophys. Acta.* 1778:1947–1977.
11. Taeusch, H. W., K. W. Lu, J. Goerke, and J. A. Clements. 1999. Nonionic polymers reverse inactivation of surfactant by meconium and other substances. *Am. J. Respir. Crit. Care Med.* 159:1391–1395.
12. Kobayashi, T., K. Ohta, K. Tashiro, K. Nishizuka, W. M. Chen, et al. 1999. Dextran restores albumin-inhibited surface activity of pulmonary surfactant extract. *J. Appl. Physiol.* 86:1778–1784.
13. Jensen, T. R., and K. Kjaer. 2001. Structural properties and interactions of thin films at the air-liquid interface explored by synchrotron x-ray scattering. *In* Novel Methods to Study Interfacial Layers. D. Möbius and R. Miller, editors. Elsevier Science, Amsterdam. 205–254.
14. Kaganer, V. M., H. Mohwald, and P. Dutta. 1999. Structure and phase transitions in Langmuir monolayers. *Rev. Mod. Phys.* 71:779–819.
15. Zuo, Y. Y., S. M. Takayyon, E. Keaing, L. Zhao, R. A. Veldhuizen, et al. 2008. Atomic force microscopy studies of functional and dysfunctional pulmonary surfactant films, II. Albumin-inhibited surfactant films and the effects of SP-A. *Biophys. J.* 95:2779–2791.
16. Braun, A., P. C. Stenger, H. E. Warriner, J. A. Zasadzinski, K. W. Lu, et al. 2007. A freeze-fracture transmission electron microscope and small angle x-ray diffraction study of the effects of albumin, serum and polymers on clinical lung surfactant microstructure. *Biophys. J.* 93:123–139.
17. Bernhard, W., J. Mottaghian, A. Gebert, G. A. Rau, H. von der Hardt, et al. 2000. Commercial versus native surfactants–surface activity, molecular components, and the effect of calcium. *Am. J. Respir. Crit. Care Med.* 162:1524–1533.
18. Als-Nielsen, J., D. Jaquemain, K. Kjaer, F. Leveiller, M. Lahav, et al. 1994. Principles and applications of grazing incidence x-ray and neutron scattering from ordered molecular monolayers at the air-water interface. *Phys. Rep.* 246:252–313.
19. Kjaer, K. 1994. Some simple ideas on x-ray reflection and grazing-incidence diffraction from thin surfactant films. *Physica B (Amsterdam).* 198:100–109.
20. Miller, C. E., J. Majewski, T. Gog, and T. L. Kuhl. 2005. Grazing incidence diffraction of cadmium arachidate multilayers at the solid-liquid interface. *Z. Kristallogr.* 220:987–992.
21. Pederson, J. S., and I. W. Hamley. 1994. Analysis of neutron and x-ray reflectivity data by constrained least-squares methods. *Physica B (Amsterdam).* 198:16–23.
22. Pederson, J. S., and I. W. Hamley. 1994. Analysis of neutron and x-ray reflectivity data I. Theory. *J. Appl. Cryst.* 27:29–35.
23. Pederson, J. S., and I. W. Hamley. 1994. Analysis of neutron and x-ray reflectivity data II. Constrained least squares methods. *J. Appl. Cryst.* 27:36–49.
24. Lee, K. Y. C., A. Gopal, A. von Nahmen, J. A. Zasadzinski, J. Majewski, et al. 2002. Influence of palmitic acid and hexadecanol on the phase transition temperature and molecular packing of dipalmitoylphosphatidyl-choline monolayers at the air-water interface. *J. Chem. Phys.* 116:774–783.
25. Bringezu, F., J. Q. Ding, G. Brezesinski, and J. A. Zasadzinski. 2001. Changes in model lung surfactant monolayers induced by palmitic acid. *Langmuir.* 17:4641–4648.
26. Alonso, C., T. Alig, J. Yoon, F. Bringezu, H. Warriner, et al. 2004. More than a monolayer: relating lung surfactant structure and mechanics to composition. *Biophys. J.* 87:4188–4202.
27. Alonso, C., F. Bringezu, G. Brezesinski, A. J. Waring, and J. A. Zasadzinski. 2005. Modifying calf lung surfactant by hexadecanol. *Langmuir.* 21:1028–1035.
28. Reference deleted in proof.
29. Wu, G., J. Majewski, C. Ege, K. Kjaer, M. Weygand, et al. 2005. Interaction between lipid monolayers and poloxamer 199: an X-ray reflectivity and diffraction study. *Biophys. J.* 89:3159–3173.
30. Lu, J. R., T. J. Su, and J. Penfold. 1999. Adsorption of serum albumin at the air/water interface. *Langmuir.* 15:6975–6983.
31. McClellan, S. J., and E. I. Franses. 2003. Effect of concentration and denaturation on adsorption and surface tension of bovine serum albumin. *Coll. Surf. B. Biointerfaces.* 28:63–75.
32. Perriman, A. W., M. J. Henderson, S. A. Holt, and J. W. White. 2007. Effect of the air-water interface on the stability of β-lactoglobulin. *J. Phys. Chem. B.* 111:13527–13537.
33. Ding, J. Q., I. Doudevski, H. E. Warriner, T. Alig, and J. A. Zasadzinski. 2003. Nanostructure changes in lung surfactant monolayers induced by interactions between palmitoyloleoylphosphatidylglycerol and surfactant protein B. *Langmuir.* 19:1539–1550.
34. Lee, K. Y. C., J. Majewski, T. L. Kuhl, P. B. Howes, K. Kjaer, et al. 2001. Synchrotron X-ray study of lung surfactant specific protein SP-B in lipid monolayers. *Biophys. J.* 81:572–585.
35. Takamoto, D. Y., M. M. Lipp, A. von Nahmen, K. Y. C. Lee, A. J. Waring, et al. 2001. Interaction of lung surfactant proteins with anionic phospholipids. *Biophys. J.* 81:153–169.
36. Wu, G., J. Majewski, C. Ege, K. Kjaer, M. Weygand, et al. 2004. Lipid corralling and poloxamer squeeze out in membranes. *Phys. Rev. Lett.* 93:028101–028104.
37. Safran, S. A., T. L. Kuhl, and J. N. Israelachvili. 2001. Polymer-induced membrane contraction, phase separation, and fusion via Marangoni flow. *Biophys. J.* 81:659–666.